Journal of Alloys and Compounds 508 (2010) 565–569

Contents lists available at ScienceDirect

Journal of Alloys and Compounds

journal homepage: www.elsevier.com/locate/jallcom

Structural and magnetic susceptibility characteristics of $Mn_{1-x}Cu_xFe_2O_4$ ($x = 0$–0.4) nanoparticles synthesized by self-assembling confined media of reverse micelle

Ali Ghasemi [a,*], Ebrahim Ghasemi [b]

[a] Materials Engineering Department, Malek Ashtar University of Technology, Shahin Shahr, Iran
[b] Department of Materials Science and Engineering, Islamic Azad University-Majlesi Branch, Majlesi Town, Iran

ARTICLE INFO

Article history:
Received 7 June 2010
Received in revised form 20 August 2010
Accepted 25 August 2010
Available online 22 September 2010

Keywords:
Ferrite
Magnetic properties

ABSTRACT

$Mn_{1-x}Cu_xFe_2O_4$ ($x = 0$–0.4) ferrite nanoparticles were prepared by reverse micelle process. X-ray diffraction (XRD), transmission electron microscopy (TEM) and vibrating sample magnetometer (VSM) were employed to probe structural and magnetic properties of samples. The temperature dependence of blocking temperature was measured using Superconducting Quantum Interference Device (SQUID) and AC magnetic susceptibility. The phenomenological Néel–Brown and Vogel–Fulcher models were employed to distinguish between the interacting or non-interacting system. Results exhibited that there is strong interaction between fine particles.

1. Introduction

Precipitation in reverse micelles is a very promising technique to prepare nanoparticles at a low temperature with narrow distribution of the size. In this process, self-assembling media of reverse micelles leads to synthesis nanoparticles of ferrite [1,2]. Briefly, reverse micelles are water-in-oil microemulsions in which molar ratio of constitutive components and pH control the size of water pools and resultant particles [2,3]. There are several literatures about the synthesizing of Ni–Zn and Mn–Zn ferrite with reverse micelle method [4,5].

Recently, we have focused our studies on the preparation and magnetic characteristics of ferrite nanoparticles [6–10]. Manganese ferrite has a cubic spinel structure and is widely used in many electronic devices because of high electrical resistivity, hard mechanical properties, high Curie temperature, and environmental stability. To the best of our knowledge no studies on the preparation of $Mn_{1-x}Cu_xFe_2O_4$ ferrite via reverse micelle method have been reported. With this view in mind, current interest is to make $Mn_{1-x}Cu_xFe_2O_4$ ferrite nanoparticles using reverse micelle technique at a low temperature and to realize the role of copper on the structural and magnetic characteristics of Mn-ferrite. Since precipitation in reverse microemulsions has been shown to be a very promising technique for the preparation of ultrafine ferrite particles of controlled size and morphology, this technique was selected in the current research.

2. Materials and methods

$Mn_{1-x}Cu_xFe_2O_4$ nanoparticles were prepared by a reverse micelle process. In the preparation of ferrites, two microemulsions were synthesized. The first, using a metal solution and the second one, using ammonium hydroxide. Stock solutions of 0.5 M sodium dioctylsulfosuccinate (AOT) were prepared in isooctane. A metal solution was synthesized using $FeCl_2$, $CuCl_2$ and $MnCl_2$ dissolved in 8 ml of water and 66 ml of AOT-isooctane. The second microemulsion was prepared by mixing 2 ml of ammonia, 2 ml of water and 66 ml of AOT-isooctane. The second microemulsion was then added to the first one and stirred for one hour at room temperature. After rapid magnetic stirring, methanol was used to extract the surfactant and organic solvent. The colloidal precipitate was sedimented by centrifuging and washing with methanol and water. To obtain spinel ferrite in the final product, the pH must be carefully controlled. The pH was adjusted to 10.3 in this experiment.

X-ray powder diffraction was performed on the nanoparticles using a Phillips X-ray diffractometer employing Cu Kα radiation from a sealed tube (50 kV, 30 mA) source. A JEOL 2010 model TEM was employed to characterize the morphologies and particle size distribution of the prepared samples. The vibrating sample magnetometer was employed to investigate the variation of magnetization with magnetic field. Magnetization versus temperature under an applied field of 115Oe was measured with a Superconducting Quantum Interference Device (SQUID). The temperature dependence of the magnetic susceptibility at different frequency ranges using Lake Shore magnetic susceptometer model 7000.

3. Results and discussions

3.1. Structural evaluations

Fig. 1 exhibits the XRD patterns of ferrite nanoparticles with composition of $x = 0$, 0.2 and 0.4. It was found from the patterns that

* Corresponding author. Tel.: +98 312 5912437; fax: +98 312 5912437.
E-mail address: ali13912001@yahoo.com (A. Ghasemi).

0925-8388/$ – see front matter © 2010 Elsevier B.V. All rights reserved.
doi:10.1016/j.jallcom.2010.08.122

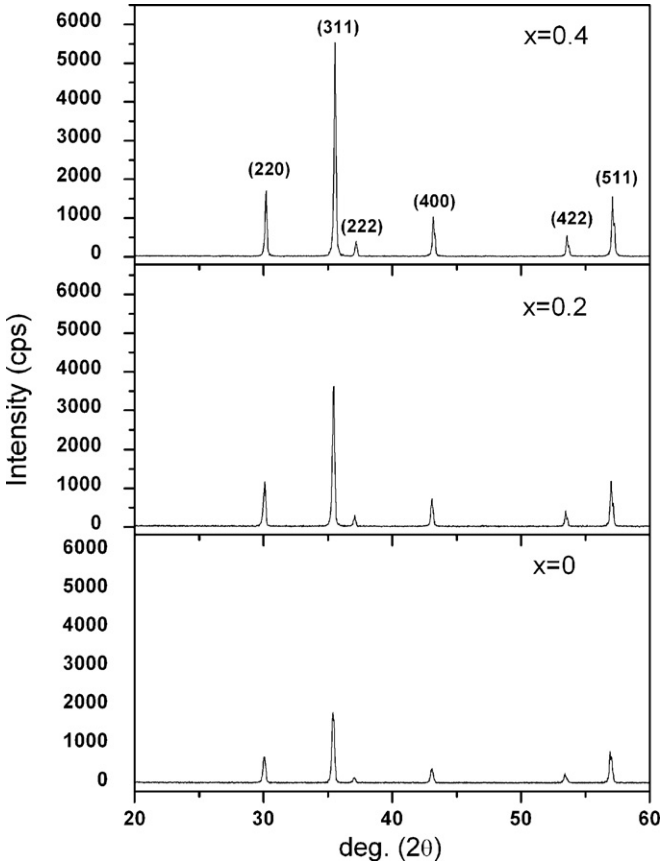

Fig. 1. XRD patterns of samples $x = 0$, 0.2 and 0.4.

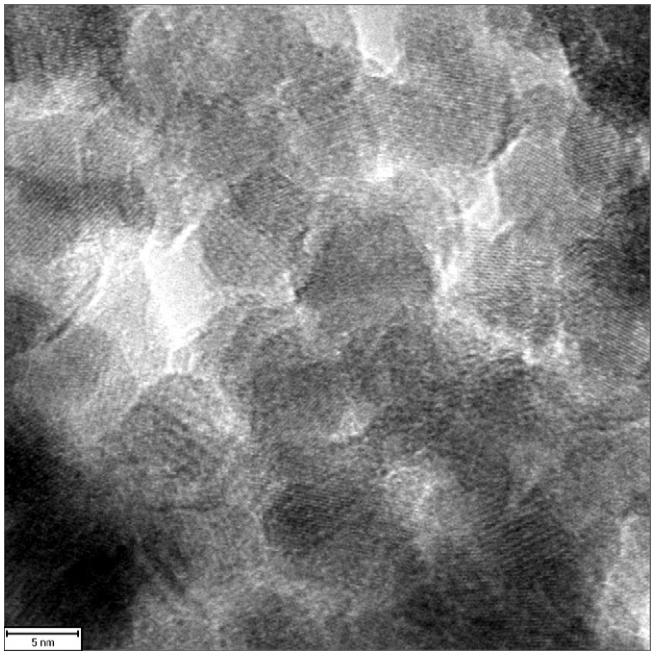

Fig. 2. TEM micrograph of sample $x = 0$.

the spinel phases can be formed in all the specimens without the existence of any secondary phases at relatively low temperature. The mean particle size was calculated from the peak broadening in X-ray powder diffraction pattern by using Williamson–Hall method [11]. The calculated values are presented in Table 1. The particle size distribution was also estimated based on analyzing the bright field images of randomly selected nanoparticles. Fig. 2 reflects the typical TEM micrographs of sample $x = 0$. The size of nanoparticles is obtained by counting 100 single nanoparticle at various micrographs. Table 1 reflects the ranges of particle size based on TEM observation. The control of particle size formed with reverse micelle method is dependent on the size of water pools of microemulsion. The main parameter influence on the water pools size is water-to-oil ratio. There are several factors including the buffering capacity of surfactant, oxidation rate, and the solubility of cations across the range of pH, which can affect the size of the final product.

The average of magnetic size can be estimated from the slope of the magnetization curve near the zero field. As pointed in the literature [12], the major contribution near zero field for superparamagnetic particles with size distribution come from the largest particles, and hence, an upper bound for the magnetic size may be estimated. According to the equation in the ref. [12].

$$d_{\max} = \left[\frac{18kT}{\pi}\frac{(dM/dH)_{H=0}}{\rho M_S^2}\right]^{1/3} \quad (1)$$

where k is the Boltzmann constant, T is the temperature (300 K), ρ is the density of prepared samples, dM/dH is the slope near zero field and M_S is the saturation magnetizations of nanoparticles. It is clear from Table 1 that the values obtained based on the Eq. (1) are smaller than those of characterized by TEM micrographs. The smaller values of the calculated magnetic particle sizes compared to the TEM observation may be an indication for the presence of a magnetically dead layer on the surface of each of the particles. This dead layer may substantially reduce the saturation magnetization of the nanocrystalline samples, as compared to that of the bulk material. This is likely to be associated with the surface effects arising from the broken exchange interactions and reduced coordination in the smaller particles. The crystallite size of ferrite obtained via reverse micelle is significantly smaller than that obtained by sol–gel process, oxalate precursor method, and co-precipitation technique. The size distribution of sol–gel final products is also wider compared to microemulsion technique.

3.2. Magnetic properties

Fig. 3 shows the room temperature hysteresis loop plots for the samples prepared via reverse micelle. Interestingly, it has been revealed from the loop that the coercivity and remanence are almost zero for all samples. The samples were not saturated even at magnetic field of 20 kOe, which shows the characteristic of superparamagnetism. The variation of magnetization of ferrite nanoparticles prepared by reverse micelle, up to a specific mag-

Table 1
The size of nanoparticles obtained from different approaches.

	$x = 0$	$x = 0.1$	$x = 0.2$	$x = 0.3$	$x = 0.4$	$x = 0.5$
TEM (nm)	6–9	10–14	13–18	19–23	22–27	26–32
XRD (nm)	4	8	12	17	20	22
Magnetization curves (nm)	3	6	11	15	18	20

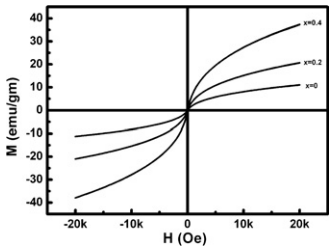

Fig. 3. VSM graphs represent the superparamagnetic trend in the nanoparticle.

Table 2
The values of coercivity and saturation magnetization of ferrite nanoparticles.

	$x=0$	$x=0.1$	$x=0.2$	$x=0.3$	$x=0.4$	$x=0.5$
M_S (emu/g)	22	29	35	41	46	51
H_C (Oe)	0.02	0.01	0.04	0.03	0.05	0.02

netic field, the magnetic moments of core align with applied field. Beyond that field, any increase in the magnetic field has an effect on the shell of the particles and therefore the slope in the increasing of magnetization slows down. The values of saturation magnetization of nanoparticles obtained by fitting the high field data to the function $M = M_S(1 - \alpha/H)$, where M and M_S are magnetization at the field H and saturation magnetization respectively, α is the fitting parameter and H is the applied field are presented in Table 2.

The lower values of saturation magnetization of nanocrystalline ferrite prepared by reverse micelle compared to the bulk ferrite (85 emu/gm) is attributed to the surface effects which leads to the non-collinearity of the magnetic moments on their surface and can be explained in terms of core–shell model of nanoparticles in which the core contains ferrimagnetically aligned spin and the surface or interface with a certain degree of spin canting. The disordering in the shell is caused due to local chemical disorder, broken exchange bonds and different local symmetry for those atoms near the surface [13]. Some researchers report that this partially disordered layer gives rise to a spin canting due to the imbalance of ferromagnetic sublattice [14,15]. However, other authors claimed that the spin canting involves the whole particle and is not restricted to the surface layer [16]. The vacancies or modified cation distribution weakens the super-exchange paths and therefore causes the spin canting in the core of ferrite nanoparticles. It must be noted that if the surfactant molecules from reverse micelle method are absorbed on the surface of nanoparticles and the electrons can no longer participate in the super-exchange interaction, then the pinning of spin occurs [17].

3.3. Interacting or non-interacting nanoparticles?

Slow dynamics in nanoparticle systems can be classified into two kinds. The first one is due to the broad distribution of relaxation times originating solely from the anisotropy energy barriers. In this non-interacting case, the magnetic moment of each particle relaxes according to its individual energy barrier that depends on the magnetic anisotropy, which in turn depends on the volume of the nanoparticle. Therefore, a distribution of particle volumes results in a distribution of energy barriers and blocking temperatures. In the second kind of slow dynamics in dense magnetic nanoparticle systems, accompanied by frustration caused by the strong dipolar interactions among the particles. In order to investigate the interacting or non-interacting behavior in the fine particle, the blocking temperatures of the prepared ferrites were characterized by ZFC-FC curves. Fig. 4 shows temperature dependence of magnetization for samples $x = 0$, 0.2 and 0.4. The ZFC curves indicate that the prepared nanoparticles exhibit crystallite size distribution. There is a

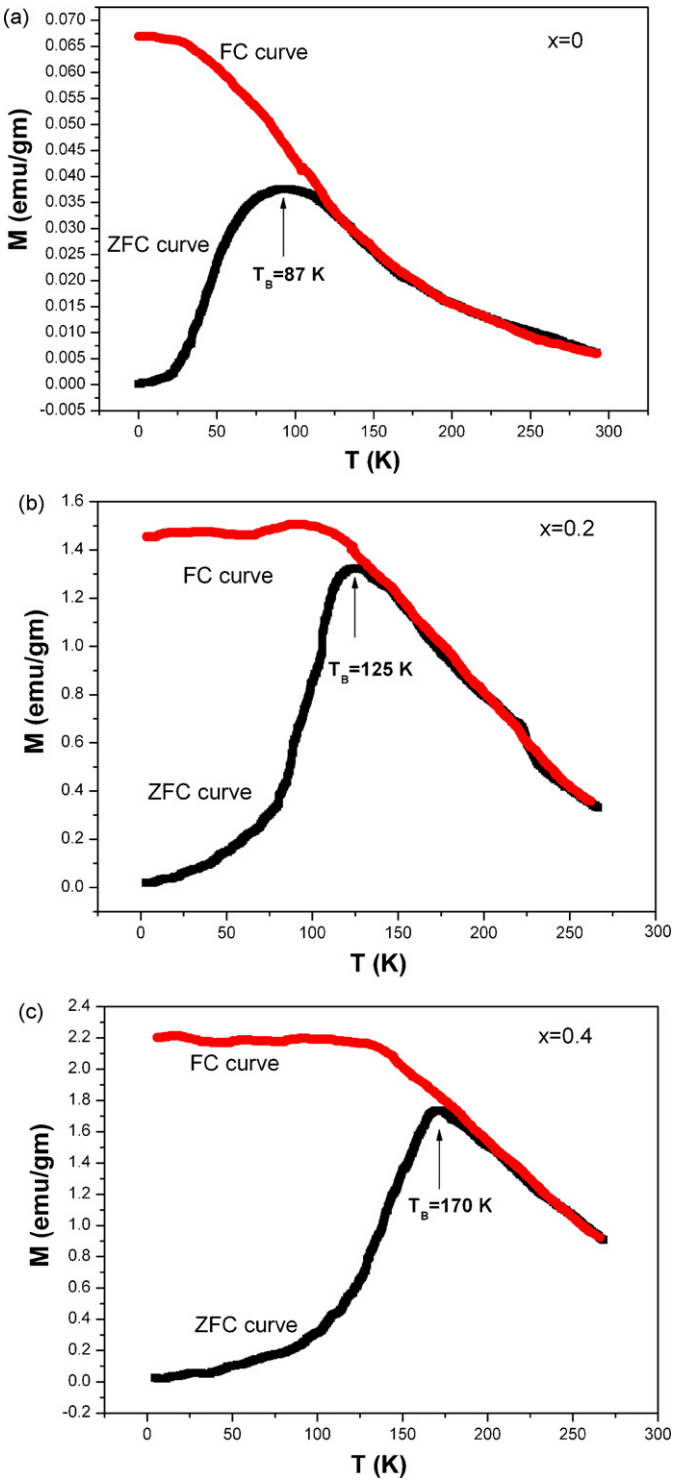

Fig. 4. ZFC-FC curves of samples $x = 0$, 0.2 and 0.4.

maximum in the ZFC curve which indicates the value of blocking temperature. Below blocking temperature, when the nanoparticles are cooled without applying the magnetic field, the magnetic moments of each single particle align in the easy axis. Considering that the measured samples are in powder configuration, random orientation of easy axes among the nanoparticles is present and the magnetization from each particle is canceled out at low temperatures. Consequently, the overall magnetization is small at low temperatures. It must be noted that the weak applied field (115 Oe) is not able to overcome the anisotropy barrier. With an increase

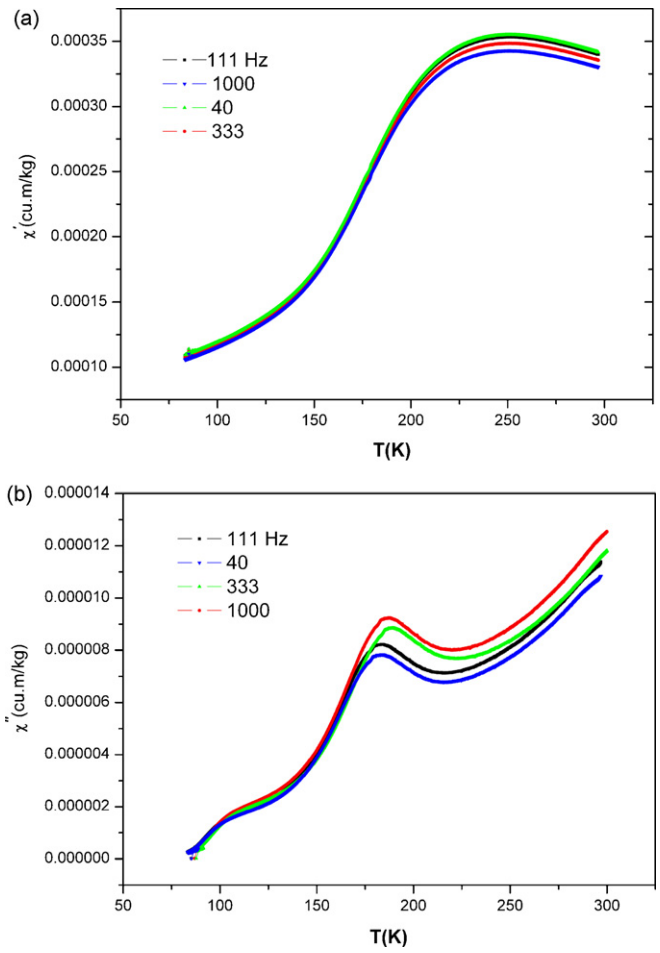

Fig. 5. Thermal variation of (a) real and (b) imaginary parts of effective magnetic susceptibility of sample $x = 0.4$.

in temperature, the thermal energy of nanoparticles increases and the magnetic moments of each particle can follow the direction of applied field, therefore the net magnetization increases. At temperatures higher than T_B, the anisotropy energy is overcome by thermal energy and the magnetization of each single particle starts to randomly flip. As a result the nanoparticles become superparamagnet. It is revealed from the graphs that with an increase in copper content, blocking temperature for the fine particle increases from 87 to 170 K. It is well known that blocking temperature is strongly dependent on particles size. Since an increase in sintering temperature leads in particle growth, consequently the blocking temperature is changed straightforwardly with size of particles. The FC curve for the sample $x = 0$ is monotonically increased with decreasing temperature and finally at 25 K, it becomes flat, while, that for the samples $x = 0.2$ and 0.4 is nearly flat below 100 and 125 K, respectively. These trends indicate the existence of strong magnetic interaction between nanoparticles.

To study the magnetic dynamic behavior of the nanoparticles, we measured the AC magnetic susceptibility of prepared ferrite nanoparticle versus temperature at different frequencies. Fig. 5 reflects the temperature dependence of real and imaginary parts of AC magnetic susceptibility of sample $x = 0.4$ at different frequencies in the range of 111–1000 Hz and at an AC magnetic field of 115 Oe. In Fig. 5, imaginary part of susceptibility reflects a peak near 175 K which is frequency dependent and shifted to a higher temperature with increasing frequency. It is worth noting that the values of blocking temperature obtained by ZFC and AC susceptibility are close together. This characteristic maximum is the signature of blocking/freezing process of the superparamagnetic/spin glass systems [18–20]. The blocking temperature is the threshold point of thermal activation. Above blocking temperature magnetocrystalline anisotropy is overcome by thermal activation and the magnetization direction of each nanoparticle simply follows the applied field direction. Consequently, the nanoparticles show paramagnetic properties. Below the blocking temperature, thermal activation is no longer able to overcome the magnetocrystalline anisotropy of the nanoparticles. As a consequence, the magnetization direction of each nanoparticle rotates from the field direction back to its own easy axis without any movement of the nanoparticle. Since the nanoparticles and consequently their easy axes are randomly orientated, overall susceptibility is reduced with decreasing temperature as shown in Fig. 5. The interacting or non-interacting behavior of the fine powders was evaluated by Neél–Brown (non-interacting model) and Vogel–Fulcher (interacting law). According to Neél–Brown model, the blocking temperature measured at a given working frequency, is related to the considered frequency as

$$\ln\left(\frac{1}{2\pi\nu}\right) = \ln\tau_0 + \frac{KV}{kT_B} \tag{2}$$

T_B can be obtained by assuming that at the maximum of the out-of-phase component of the susceptibility, the relaxation time matches the working frequency [21–23]. Attempt time is calculated from the curves and it is found that it spreads between $\tau_0 = 10^{-27}$ to 10^{-25} s. These values, however, are unphysical, being several orders of magnitude lower than the typical value found in the literature for a non-interacting assembly of superparamagnetic nanoparticles (10^{-8} to 10^{-11} s) [18]. This suggests that the Neél–Brown model is not appropriate to describe the dynamic behavior of our system. In this case, deviations from the model can be ascribed to the presence of strong interactions. The interaction between nanoparticles affected the blocking/freezing temperature by modifying the potential barrier. By increasing the strength of interaction, T_B shifts to higher temperatures. For interacting magnetic nanoparticles, the frequency dependence of T_B is given by the Vogel–Fulcher law [18].

$$\ln\left(\frac{1}{2\pi\nu}\right) = \ln\tau_0 + \frac{E_a}{k(T - T_0)} \tag{3}$$

here E_a is the energy of barrier, T_0 is an effective temperature which reveals the existence of the interaction between nanoparticles and T is the characteristic temperature indicating the onset of the blocking process. We tried to fit the experimental data of susceptibility for our samples, using Eq. (3). It was found that the values of attempt time were spread between 2.7×10^{-9} to 5.6×10^{-10} s. The good agreement between the experimental data and Vogel–Fulcher model confirms the existence of strong interactions between nanoparticles.

4. Conclusions

Fine particles single phase of spinel phase are prepared by reverse micelle method. The value of calculated saturation magnetization for fine particles is much lower than that of large particles. This behavior can be explained by core–shell model. The value of blocking temperature has straightforward relation with particle size. Temperature dependence of real and imaginary parts of effective magnetic susceptibility was measured. Fitting the experimental data of susceptibility with Neél–Brown model gives unphysical high values for relaxation time and indicates that there are strong interactions between nanoparticles of ferrite. The good agreement between the experimental data and Vogel–Fulcher model confirms the existence of strong interactions between nanoparticles.

References

[1] S. Thakur, S.C. Latyal, M. Singh, J. Magn. Magn. Mater. 321 (2009) 1–7.
[2] V. Uskokovic, M. Drofenik, I. Ban, J. Magn. Magn. Mater. 284 (2004) 294–302.
[3] M.D. Shultz, M.J. Allsbrook, E.E. Carpenter, J. Appl. Phys. 101 (2007), 09M518–09M521.
[4] S.A. Morrison, C.L. Cahill, E.E. Carpenrer, S. Calvin, R. Swaminathan, M.E. McHenry, V.G. Harris, J. Appl. Phys. 95 (2004) 6392–6396.
[5] S.A. Morrison, C.L. Cahill, E.E. Carpenrer, S. Calvin, V.G. Harris, J. Appl. Phys. 93 (2003) 7489–7492.
[6] A. Ghasemi, V. Šepelák, X.X. Liu, A. Morisako, J. Appl. Phys. 107 (2010), 09A734–09A737.
[7] A. Ghasemi, V. Šepelák, X.X. Liu, A. Morisako, A. Ghasemi, J. Appl. Phys. 107 (2010), 09A743–09A746.
[8] A. Ghasemi, V. Šepelák, X.X. Liu, A. Morisako, IEEE Trans. Magn. 45 (2009) 2456–2460.
[9] A. Ghasemi, X. Liu, A. Morisako, IEEE Trans. Magn. 45 (2009) 4420–4424.
[10] A. Ghasemi, A. Morisako, J. Magn. Magn. Mater. 320 (2008) 1167–1172.
[11] G.K. Williamson, W.H. Hall, Acta Metall. 1 (1953) 22–31.
[12] I. Yaacob, A. Nunes, A. Bose, D. Shah, J. Colloid Interface Sci. 168 (1994) 289–301.
[13] E. Tronc, D. Fiorani, M. Noguès, A.M. Testa, F. Lucari, F. D'Orazio, J.M. Grenèche, W. Wernsdorfer, N. Galvez, C. Chanéac, D. Mailly, J.P. Jolivet, J. Magn. Magn. Mater. 262 (2003) 6–14.
[14] E. Tronc, A. Ezzir, R. Cherkaoui, C. Chanéac, M. Noguès, H. Kachkachi, D. Fiorani, A.M. Testa, J.M. Grenèche, J.P. Jolivet, J. Magn. Magn. Mater. 221 (2000) 63–79.
[15] J.Z. Jiang, G.F. Goya, H.R. Rechenberg, J. Phys.: Condens. Matter. 11 (1999) 4063–4078.
[16] V. Šepelák, Am. Chim. Sci. Mater. 27 (2002) 61–76.
[17] S. Linderoth, M.S. Pedersen, J. Appl. Phys. 35 (2002) 3035–3038.
[18] J.L. Dormann, D. Fiorani, D. Tronc, J. Magn. Magn. Mater. 202 (1999) 251–267.
[19] P.E. Jönsson, Adv. Chem. Phys. 128 (2004) 191–248.
[20] M. Suzuki, S.I. Fullem, I.S. Suzuki, Phys. Rev. B 79 (2009) 024418–024425.
[21] D. Parker, V. Dupuis, F. Ladieu, J.P. Bouchaud, E. Dubois, R. Perzynski, E. Vincent, Phys. Rev. B 77 (2008) 104428–104437.
[22] S. Vasseur, E. Duguet, J. Portier, G. Goglio, S. Mornet, E. Hadová, K. Knížek, M. Maryško, P. Veverka, E. Pollert, J. Magn. Magn. Mater. 302 (2006) 315–320.
[23] G.F. Goya, T.S. BerquÓ, F.C. Fonseca, M.P. Morales, J. Appl. Phys. 94 (2003) 3520–3529.